Theoretical and Applied Climatology
https://doi.org/10.1007/s00704-022-04306-y

RESEARCH

Evaluation of ERA5 reanalysis over the deserts in northern China

Chengzhi Hou[1] · Danqing Huang[2] · Hao Xu[3,4] · Zhiwei Xu[1]

Received: 5 July 2022 / Accepted: 23 November 2022

Abstract
Deserts cover a vast area of the world's land surface, but the study of desert climate has been impeded by the lack of ground meteorological observations. In recent years, the climate reanalysis products provide an important data source to investigate climate change in observation-limited areas. However, their accuracy in desert regions has been poorly investigated. Here, we evaluated the performance of the latest ERA5 reanalysis datasets for the climatic conditions over the deserts of northern China (DNC), including temperature and precipitation variations, climate extremes, and detection skills of daily precipitation. The results show that ERA5 well captures the observed pattern of annual and seasonal temperatures, as well as the warming trend during the past four decades in DNC, compared to the ground observations. However, both annual and seasonal precipitations are greatly overestimated over DNC, and large uncertainties exist in precipitation trends. In addition, the variability of interannual precipitation, precipitation intensity, maximum 1-day precipitation, and the number of continuous dry days are underestimated by ERA5. The bias of precipitation estimates may be traced to the overestimation of rainfall occurrence in ERA5. Comparing to other reanalysis (such as MERRA2, NCEP/NCAR, and NOAA-20C), the ERA5 outperforms them for precipitation and precipitation extremes over DNC, although its performance is not as good as gridded gauge-based precipitation datasets (such as CPC). Overall, this study provides references for the use of ERA5 over DNC and facilitates the applications of ERA5 over other observation-limited desert regions.

Keywords ERA5 reanalysis · Deserts of northern China · Desert climate · Climate extremes · Rainfall occurrence

1 Introduction

Deserts are characterized by dry climate and bare ground with sparse vegetation and distributed extensively in the world's arid regions. Desert climate is a specific climate type in the Köppen climate classification system and is characterized by large variability in both temperature and precipitation (Peel et al. 2007). For instance, most deserts have large diurnal temperature fluctuations due to very dry air condition (Malek and Bingham 1997). Precipitation in the deserts is scarce but has strong interannual variability (Thomas and Shaw 1991). One heavy rainfall event may account for more than half of annual amount of precipitation in some desert regions (Kampf et al. 2018). More importantly, deserts are ecologically fragile and sensitive to climate change and human activities. The fluctuation of climate conditions can have great impacts on desert ecosystems, as well as the activity of sand dunes which are widely distributed in the deserts (Xu et al. 2018), and may lead to land desertification (Wang et al. 2017). Meanwhile, changes in the desert ecosystems and environments would have strong feedbacks to the atmosphere by modifying boundary layer conditions (Charney 1975; Kucharski et al. 2013) or even broader impact through dust emissions (Kim et al. 2017; Wang et al. 2021).

Despite of the important role of deserts in the Earth system, ground observations are relatively lack in these regions due to their remote geographical locations (He and

✉ Danqing Huang
huangdq@nju.edu.cn

✉ Zhiwei Xu
zhiweixu@nju.edu.cn

[1] School of Geography and Ocean Science, Nanjing University, Nanjing, China

[2] School of Atmospheric Sciences, Nanjing University, Nanjing, China

[3] Institute of Forestry and Grassland Ecology, Ningxia Academy of Agricultural and Forestry Sciences, Yinchuan, China

[4] Ningxia Key Laboratory of Desertification Control and Soil and Water Conservation, Yinchuan, China

Published online: 03 December 2022

Jin 2021). In such a case, climate reanalysis products which provide spatially distributed meteorological information are especially valuable for those areas where ground meteorological stations are non-existent or scattered (Kalnay et al. 1996; Bosilovich 2013). Climate reanalysis products assimilate a wide variety of historical observations into numerical weather prediction models to generate a synthesized estimate of the state of the atmosphere (Bengtsson et al. 2007). In recent years, the applications of climate reanalysis datasets, such as the fifth-generation reanalysis recently released by the European Centre for Medium Range Weather Forecasts (ECMWF), i.e., ERA5, the National Centers for Environmental Prediction/National Centers for Atmospheric Research reanalysis (NCEP/NCAR), the Modern-Era Retrospective analysis for Research and Applications, Version 2 (MERRA2), and others, have greatly improved our understandings about recent climate changes (Hodges et al. 2011; Huang et al. 2016). However, given the uncertainty coming from the numerical prediction models, the initial conditions and data assimilation methods (Hodges et al. 2011), these reanalysis products might have certain biases, and it is necessary to evaluate their accuracy before applying them in climate change studies in different regions. Many studies have assessed the quality of reanalysis products at both global and regional scales (Bosilovich et al. 2008; Donat et al. 2014; Torralba et al. 2017). Despite that, there are fewer studies focusing on their performance in observation-limited regions (Huang et al. 2021; Huai et al. 2021), though the overestimation of rainfall occurrence in reanalysis products might be larger in the desert regions (Dinku et al. 2010).

Deserts of northern China (DNC) cover a vast area in the hinterland of Central and East Asia and have strong influences in local ecological and environmental conditions. The east part of DNC includes several semi-arid dune fields with annual precipitation greater than 200 mm, while the west part of DNC is mostly composed of large sand seas with annual precipitation less than 200 mm (Fig. 1). Among DNC, the Taklamakan desert is the second largest mobile desert in the world (He and Jin 2021). More importantly, changes in different climatic variables over DNC are dramatic in recent years, such as rapidly warming (Huang et al. 2019), and increased occurrence of precipitation extremes (Li et al. 2019). As a result, some parts of DNC have experienced widespread greening trend under wetter, warmer, and less windy conditions during past few decades (Xu et al. 2018; Wang et al. 2022). Despite of the increasing evidence showing the significant impacts of climate change in DNC, ground meteorological observations are scarce and distributed unevenly in this region, which brings much uncertainty to understand the trend and causes of climate change over DNC (Su et al. 2016; Ning et al. 2021). Reanalysis products with high spatial and temporal resolutions are potential alternatives and an important complement to ground observations in DNC. However, to our current knowledge, there are few studies evaluating the performance of reanalysis products over DNC (Huang et al. 2021), and thus, a systematic evaluation is in great need.

In this study, a comprehensive evaluation of the latest ERA5 reanalysis over DNC would be carried out. We mainly focus on ERA5 reanalysis based on the following reasons:

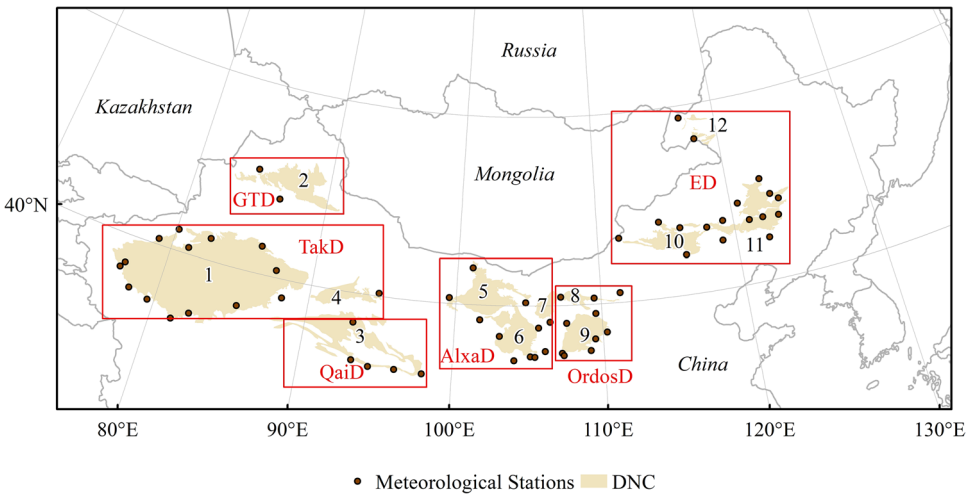

Fig. 1 Spatial distribution of DNC and meteorological stations. The shade in the map refers to the deserts and dune fields, while the dots indicate the meteorological stations. 1, Taklamakan desert; 2, Gurban Tunggut desert; 3, Qaidam desert; 4, Kumtagh desert; 5, Badain Jaran desert; 6, Tengger desert; 7, Ulan Buh desert; 8, Hobq desert; 9, Mu Us dune field; 10, Otindag dune field; 11, Horqin dune field; 12, Hulun Buir dune field. These deserts and dune fields are divided into six sub-regions based on their geographical locations and climate conditions. The box labels each sub-region. TakD, Taklamakan and Kumtagh deserts; GTD, Gurban Tunggut desert; QaiD, Qaidam desert; AlxaD, Badain Jaran, Tengger, and Ulan Buh deserts; OrdosD, Hobq desert and Mu Us dune field; ED, Otindag, Horqin, and Hulun Buir dune fields

First, ERA5 has been recently developed as the fifth-generation reanalysis and released by ECMWF (Hersbach et al. 2020). Compared with the earlier ECMWF reanalysis, i.e., ERA-Interim, two major changes were implemented in ERA5: The temporal resolution was increased from 3-hourly to hourly and the spatial resolution was also increased (Albergel et al. 2018). Second, previous studies have revealed that ERA5 has generally good performance at both global and regional scales. For example, Huai et al. (2021) have found ERA5 outperform other reanalysis datasets for most climate variables, such as temperature, air pressure, and precipitation, over Qilian Mountains, Qinghai-Tibet Plateau. Mahto and Mishra (2019) have found that ERA5 performs better than other reanalysis products (ERA-Interim, JRA-55 and MERRA2) over India region, including seasonal precipitation, maximum and minimum temperatures, total runoff, evapotranspiration, and soil moisture. Graham et al. (2019) have confirmed improved performance of ERA5 in Arctic Gateway relative to other reanalysis datasets, such as ERA-Interim, JRA-55, and MERRA2. Third, few studies have been carried out to evaluate the performance of ERA5 over DNC, though this reanalysis product may have particular advantage for further investigation of climate change and its impact in this region. In this study, the performance of ERA5 in reproducing both annual and seasonal temperatures and precipitations, as well as climate extremes, would be evaluated over DNC, in comparison to both ground observations (OBS) and other climate datasets (including MERRA2, NCEP/NCAR, NOAA-20C, PREC/L, GPCP and CPC). This study should not only become an important basis for the use of ERA5 reanalysis in DNC, but also provide insights into climate change studies in other observation-limited desert regions.

2 Study area

DNC are located in the arid and semi-arid areas of Central and East Asia and influenced by both Asian monsoon circulations and the westerlies. They consist eight large sand seas, namely Taklamakan, Gurban Tunggut, Kumtagh, Qaidam, Badain Jaran, Tengger, Ulan Buh, and Hobq deserts, and four semi-arid dune fields, namely Mu Us, Otindag, Horqin, and Hulun Buir dune fields (Fig. 1). In this study, DNC are divided into six sub-regions based on their climate conditions and geographical locations, as shown by the boxes in Fig. 1. The sand seas distributed in the west part of DNC usually have annual precipitation less than 200 mm, because the humid air from the ocean is difficult to reach. The dune fields located in the east part are strongly affected by Asian summer monsoon and have annual precipitation ranging from 200 to 450 mm. The climate characteristics of each desert or dune field are additionally affected by their specific geographical locations. The driest Taklamakan and Kumtagh deserts located in the Tarim basin are surrounded by high mountain ranges, and they have a warm climate with annual temperature higher than 10 ℃. In comparison, the Qaidam desert is located in the Tibetan Plateau and has a higher altitude and relatively low temperature. The Gurban Tunggut desert is located north to the Taklamakan desert, both of which are strongly influenced by the westerlies. The Badain Jaran, Tengger, and Ulan Buh deserts are located in the Alxa Plateau in central part of DNC. They are influenced by monsoon circulations and thus have relatively higher precipitation than other sand seas in the west. The Hobq desert and Mu Us dune field are located in the Ordos Plateau, north-central China, and they have higher precipitation than the sand seas in the Alxa Plateau. Finally, the Otindag, Horqin, and Hulun Buir dune fields are located in the east part of DNC. These dune fields are influenced by summer monsoon, and have annual precipitation ranging from 200 to more than 450 mm. Therefore, these sand seas and dune fields can be divided into six sub-regions: (1) Taklamakan Desert Region (TakD) that includes Taklamakan and Kumtagh deserts; (2) Gurban Tunggut Desert Region (GTD); (3) Qaidam Desert Region (QaiD); (4) Alxa Desert Region (AlxaD) that includes Badain Jaran, Tengger and Ulan Buh deserts; (5) Ordos Desert Region (OrdosD) that includes Hobq desert and Mu Us dune field; (6) Eastern Desert Region (ED) that includes Otindag, Horqin and Hulun Buir dune fields. Detail information of these six sub-regions is shown in Table 1.

3 Data and methodology

3.1 Data source

3.1.1 ERA5 reanalysis

As one of the latest high-resolution climate reanalysis datasets, ERA5 provides hourly estimates of a large number of atmospheric, land, and oceanic climate variables (Hersbach et al. 2020). It has a high spatial resolution up to $0.25° \times 0.25°$ and resolves the atmosphere using 137 levels from the surface up to a height of 80 km. For this study, hourly climate variables including 2 m temperature and total precipitation from the ERA5 reanalysis, spanning January 1979 to December 2019, were obtained from the Copernicus Climate Data Store. Then, daily, monthly, and annual climate variables were calculated based on hourly data.

3.1.2 Ground observations

The observation data were derived from China Meteorological Administration. The climate variables include daily mean, maximum, minimum temperature, and daily

Table 1 Information of sub-regions of DNC

Short name	Full name	Deserts/dune fields	Geographical location
TakD	Taklamakan Desert Region	Taklamakan and Kumtagh deserts	Tarim Basin south of the Tianshan Mountains
GTD	Gurban Tunggut Desert Region	Gurban Tunggut desert	Junggar Basin north of the Tianshan Mountains
QaiD	Qaidam Desert Region	Qaidam desert	Qaidam Basin in the Tibetan Plateau
AlxaD	Alxa Desert Region	Badain Jaran, Tengger and Ulan Buh deserts	Alxa Plateau west of the Helan Mountains and north of the Qilian Mountains
OrdosD	Ordos Desert Region	Hobq desert and Mu Us dune field	Ordos Plateau east of the Helan Mountains and west of the Taihang Mountains
ED	Eastern Desert Region	Otindag, Horqin and Hulun Buir dune fields	Mongolia Plateau in northeastern China

precipitation. Careful quality control was carried out first to select the observation data. Stations with missing values amounting to more than 5% of the total daily data were excluded. Finally, 60 meteorological stations that meet the quality control were selected, and their geographic locations are shown in Fig. 1.

3.1.3 Other climate datasets

Four other climate reanalysis products and three gridded gauge-based precipitation datasets were analyzed to compare with the ERA5. The reanalysis datasets include:

1. The Modern-Era Retrospective analysis for Research and Applications (MERRA2), spanning from 1980 to present with horizontal resolution of 0.5°×0.625° (Bosilovich et al. 2008).
2. NCEP/NCAR Reanalysis 1 project (NCEP1), spanning from 1948 to present with horizontal resolution of 2.5°×2.5° (Kalnay et al. 1996).
3. NCEP-US Department of Energy (DOE) Atmospheric Model Intercomparison Project II reanalysis (NCEP2), spanning from 1948 to present with horizontal resolution of 2.5°×2.5° (Kanamitsu et al. 2002).
4. NOAA-CIRES-DOE 20th Century Reanalysis V3 (NOAA-20C), spanning from 1836 to 2015 with horizontal resolution of 1.0°×1.0° (Giese et al. 2016).

The gridded precipitation datasets include:

1. NOAA's Gridded Precipitation Reconstruction over Land (PREC/L), spanning from 1948 to present with horizontal resolution of 2.5°×2.5° (Chen et al. 2002).
2. Precipitation datasets from Global Precipitation Climatology Project (GPCP), spanning from 1979 to present with horizontal resolution of 2.5°×2.5° (Huffman et al. 1997).
3. Global Daily Unified Gauge-Based Analysis of Precipitation from NOAA Climate Prediction Center (CPC), spanning from 1979 to present with horizontal resolution of 0.5°×0.5° (Xie et al. 2007).

3.2 Methodology

In this study, a point-to-pixel evaluation was carried out at each meteorological station over DNC. This method can avoid errors from interpolation and thus is widely applied in the evaluation of reanalysis products (Zhang et al. 2018). The reanalysis data from the specific grids which contain the meteorological stations would be compared with the corresponding observation data. Different statistical indices including correlation coefficient (*CC*), mean bias (*MB*), relative bias (*RB*), root-mean-square error (*RMSE*), and relative root-mean-square error (*RRMSE*) were calculated between the observation data (OBS) and the reanalysis data (ERA5, MERRA2, NCEP1, NCEP2, NOAA-20C) and between the OBS and gridded gauge-based precipitation datasets (PREC/L, GPCP, CPC). *POD*, *FAR*, and *CSI* were calculated to evaluate the capacity of ERA5 and CPC in detecting daily precipitation events (Liu et al. 2019). Formula and detailed information of these indices are displayed in Tables 2 and 3.

Considering the large variability of both precipitation and temperature in the deserts, the climatic extremes were investigated and evaluated to make a full consideration of the performance of ERA5 over DNC. Some specific indices for climate extremes that are defined by Expert Team on Climate Change Detection and Indices (ETCCDI, http://etccdi.pacificclimate.org/indices.shtml) and are relevant to the desert environments were calculated, including the coefficient of variation of annual precipitation (*CV*), the number of days with precipitation higher than 1 mm (*RD*), and so on. The definitions of these indices are explained in Table 4. Based on these indices, the performance of ERA5 in reproducing the climate extremes over DNC was evaluated.

Table 2 Information of the statistical indices used in this study. In the formula, n is the length of time series, E_i is the climate variables in ERA5 during i period, O_i is the climate variables based on ground meteorological observations, and $\overline{E}$ and $\overline{O}$ are the average value in corresponding periods

Short name	Full name	Formula
CC	Correlation coefficient	$CC = \frac{\sum_{i=1}^{n}\left(E_i-\overline{E}\right)\left(O_i-\overline{O}\right)}{\sqrt{\sum_{i=1}^{n}\left(E_i-\overline{E}\right)^2\left(O_i-\overline{O}\right)^2}}$
MB	Mean bias	$MB = \frac{1}{n}\sum_{i=1}^{n}\left(E_i - O_i\right)$
RB	Relative bias	$RB = \frac{MB}{\overline{O}}$
RMSE	Root-mean-square error	$RMSE = \sqrt{\frac{1}{n}\sum_{i=1}^{n}\left(E_i - O_i\right)^2}$
RRMSE	Relative root-mean-square error	$RRMSE = \frac{RMSE}{\overline{O}}$

Table 3 Computing formula of *POD*, *FAR*, and *CSI*, which are used to evaluate the capacity of ERA5 in detecting daily precipitation events. H is the number of hits, which means the frequency of precipitation events recorded in both ERA5 and meteorological stations. M is the number of misses, which means that the frequency of precipitation events recorded in meteorological stations but missed in ERA5. F is the number of false alarms which means the frequency of precipitation event occurring in ERA5 but not appearing in the meteorological stations

Short name	Full name	Formula
POD	Probability of detection	$POD = \frac{H}{H+M}$
FAR	False alarm ratio	$FAR = \frac{F}{H+F}$
CSI	Critical success index	$CSI = \frac{H}{H+F+M}$

4 Results

4.1 Evaluation of annual and seasonal variations

4.1.1 Spatial pattern

The consistency of annual and seasonal temperatures in DNC between the OBS and ERA5 was evaluated using *CC*, *MB*, and *RMSE*, and the results are shown in Fig. 2. For annual temperature, *CC* values across DNC are almost higher than 0.9, except for some stations in TakD with *CC* lower than 0.5 (Fig. 2a). For seasonal temperature, the averaged *CC* values for DNC as a whole exceed 0.9 in all seasons and the highest *CC* is 0.95 in spring (Fig. 3a). ERA5 shows a warm bias in 40 stations, and the highest *MB* is 1.4 ℃, while cold bias is found in 20 stations with the highest *MB* of − 3.6 ℃, mainly occurring in high-altitude regions, such as QaiD in the northeastern Tibetan Plateau and southern TakD near the Kunlun Mountains (Fig. 2f). In general, the spatial pattern of *MB* in seasonal temperature is similar with that of annual temperature (Fig. 2g-j). Most of the cold bias occur in high-altitude regions, while warm biases are found in ED, where the altitude is low and the terrain is flat. *RMSE* values of annual and seasonal temperatures mostly range from 0 to 2, except for some stations in QaiD and TakD (Fig. 2k-o). The averaged *MB* and *RMSE* in all seasons are similar to that of annual average (Fig. 3b and c).

As shown in Fig. 4, *CC* values of annual precipitation are not as high as those of annual temperature. The averaged *CC* value for the whole DNC is 0.65 (Fig. 5a). For some stations in ED and TakD, *CC* are higher than 0.7, while *CC* in most other stations range from 0.4 to 0.7 (Fig. 4a). For most stations, *CC* in spring and autumn precipitation are higher than that of summer and winter precipitation. The averaged *CC* for the whole DNC in spring is the highest among all seasons (Fig. 5a). Both annual and seasonal precipitations are overestimated across DNC, as indicated by positive *RB*

Table 4 Definitions of climate extreme indices

Indices	Unit	Definition
TX	℃	Averaged daily maximum temperature
TN	℃	Averaged daily minimum temperature
DTR	℃	Averaged daily temperature range
CV	\	Coefficient of variation of annual precipitation
SDII	mm/day	Averaged precipitation intensity of all wet days (> 1 mm)
Rx1d	mm	Maximum 1-day precipitation
CDD	days	Maximum number of consecutive days with precipitation < 1 mm
RD	days	Number of days with precipitation ≥ 1 mm

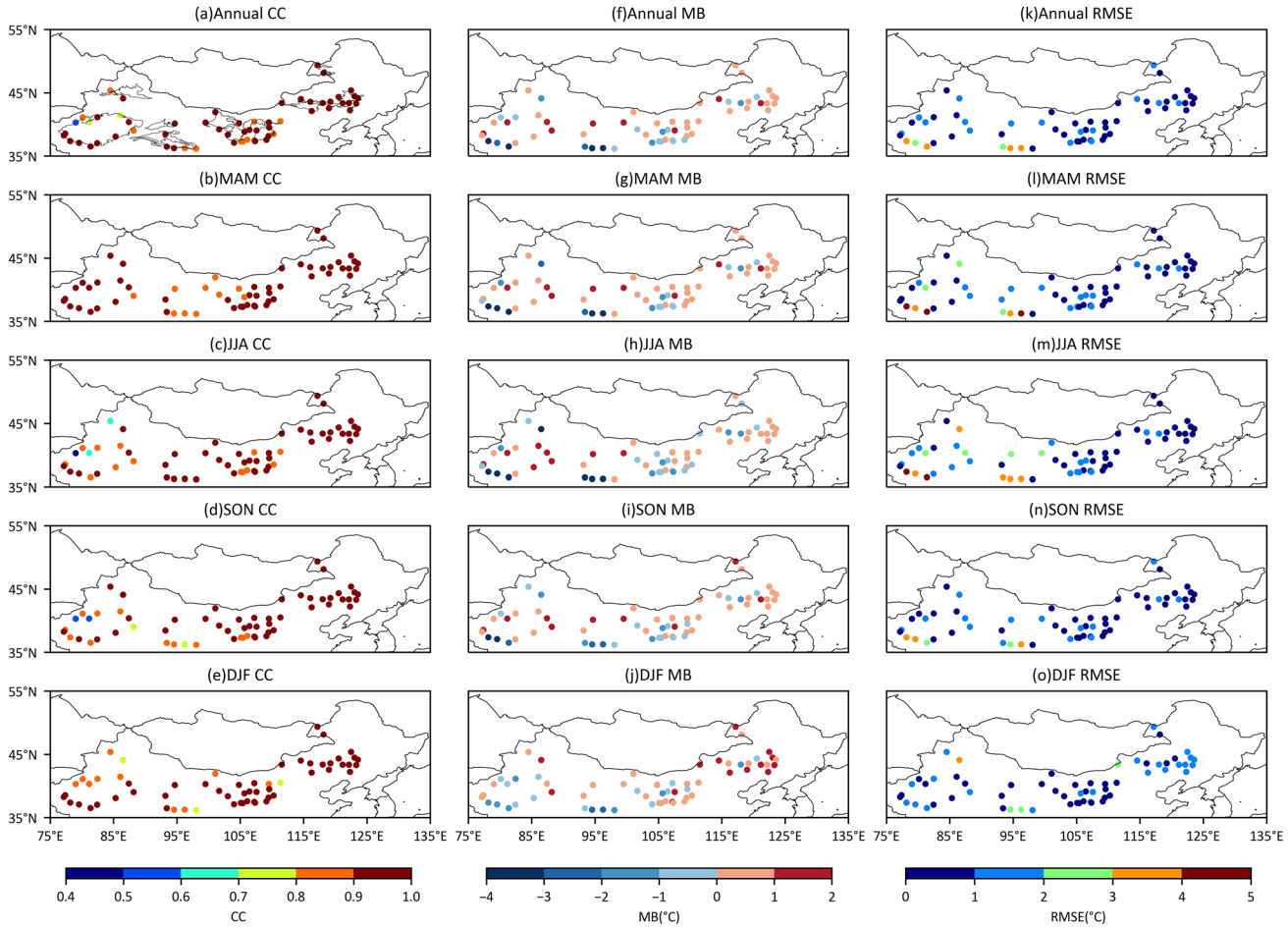

Fig. 2 Spatial distribution of statistical indices of annual and seasonal temperatures at each station. (a–e) Correlation coefficient (*CC*) between OBS and ERA5, calculated for annual, spring (MAM), summer (JJA), autumn (SON), and winter (DJF) temperature, respectively. (f–j) Mean bias (*MB*) between OBS and ERA5. (k–o) Root mean square error (*RMSE*) between OBS and ERA5. The dots represent the geographical location of each station

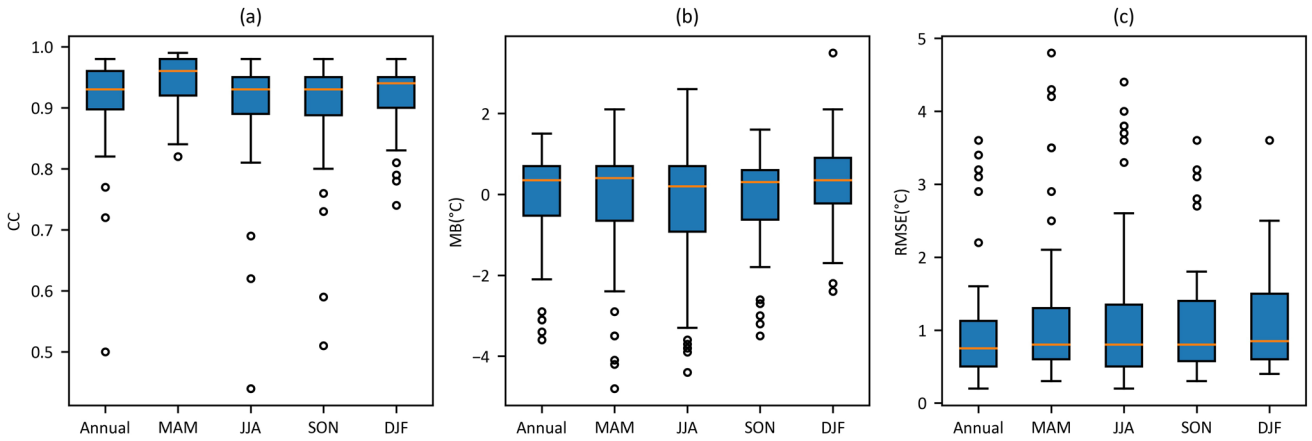

Fig. 3 Boxplot of statistical indices of annual and seasonal temperatures. **a** Correlation coefficient (*CC*) between OBS and ERA5, calculated for annual, spring (MAM), summer (JJA), autumn (SON), and winter (DJF) temperature, respectively. **b** Mean bias (*MB*) between OBS and ERA5. **c** Root mean square error (*RMSE*) between OBS and ERA5

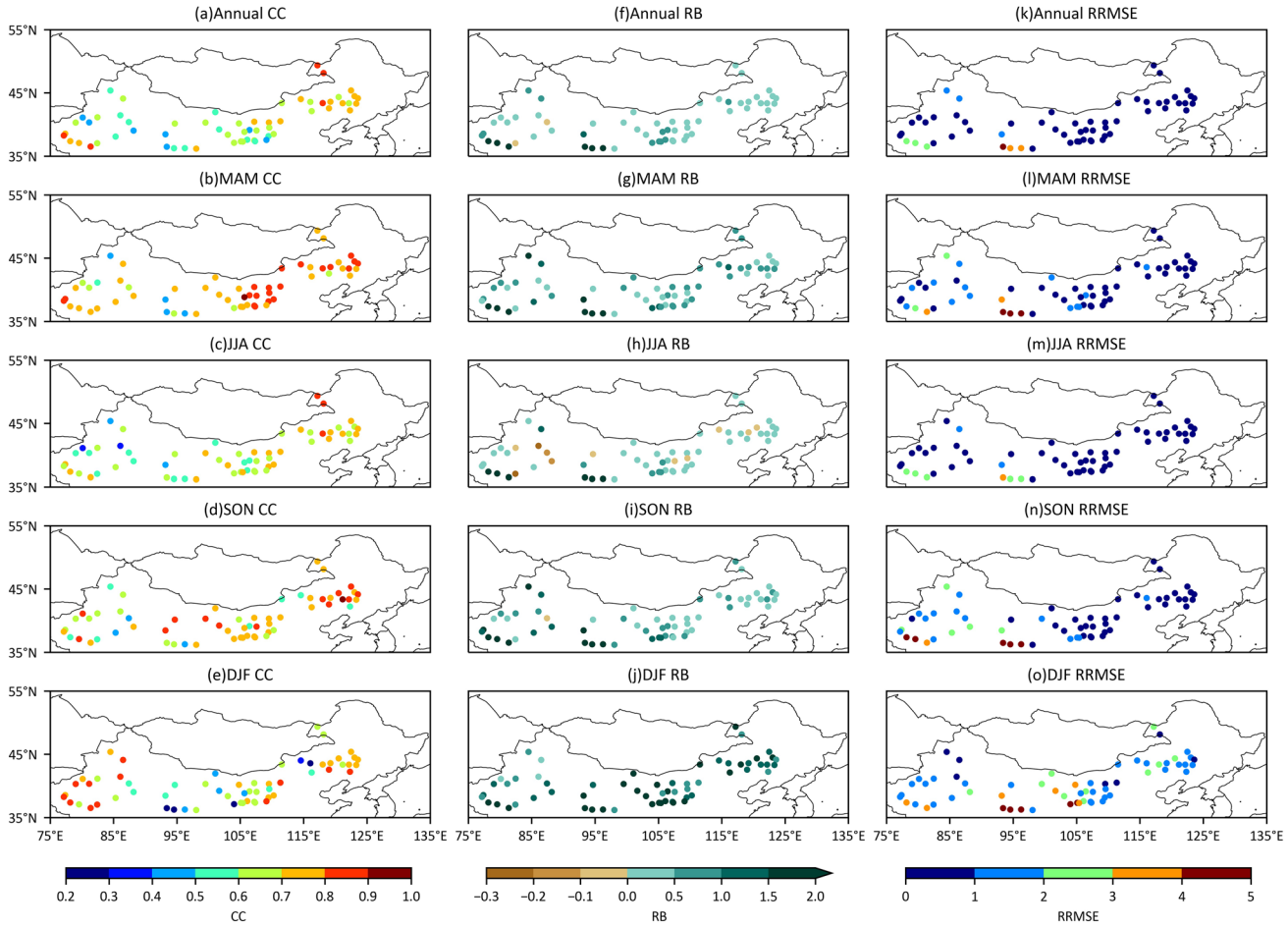

Fig. 4 Spatial distribution of statistical indices of annual and seasonal precipitations at each station. (**a**–**e**) Correlation coefficient (*CC*) between OBS and ERA5, calculated for annual, spring (MAM), summer (JJA), autumn (SON) and winter (DJF) temperature, respectively. (**f**–**j**) Relative bias (*RB*) between OBS and ERA5. (**k**–**o**) Relative root-mean-square error (*RRMSE*) between OBS and ERA5. The dots represent the geographical location of each station

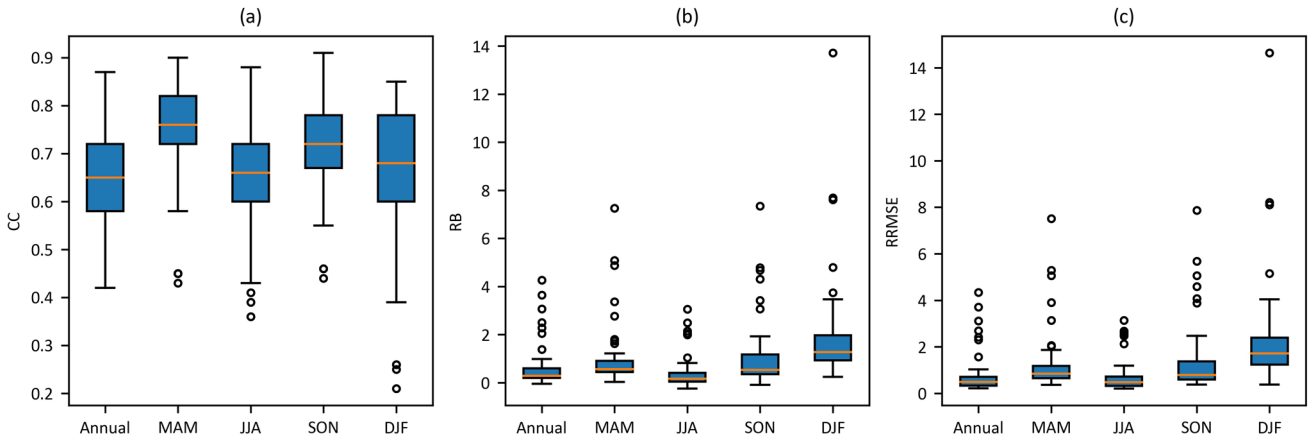

Fig. 5 Boxplot of statistical indices of annual and seasonal precipitations. **a** Correlation coefficient (*CC*) between OBS and ERA5, calculated for annual, spring (MAM), summer (JJA), autumn (SON), and winter (DJF) temperature, respectively. **b** Relative bias (*RB*) between OBS and ERA5. **c** Relative root-mean-square error (*RRMSE*) between OBS and ERA

values (Fig. 4f-j). For annual precipitation, the averaged *RB* value is 62% in DNC (Fig. 5b). The wet bias reaches even to more than 200% in the mountainous regions, such as Kunlun Mountains, Tianshan Mountains, Qilian Mountains, and Helan Mountains (Fig. 4f). For seasonal precipitation, wet bias in summer is about 40%, which is the smallest among all seasons (Fig. 5b), and summer precipitation at some stations is even underestimated in ERA5 (Fig. 4h). By contrast, winter precipitation is heavily overestimated by the ERA5, with averaged *RB* of 228% (Fig. 5b). The *RRMSE* values for annual and seasonal precipitations are relatively high in western desert regions, such as QaiD and TakD (Fig. 4k-o). As for seasonal features, *RRMSE* is the lowest in summer and the highest in winter, which is similar to *RB* (Fig. 5c).

4.1.2 Interannual variation and linear trends

The temporal variations in annual mean temperature during 1979–2019 calculated from ERA5 show good correlations with the OBS in all sub-regions of DNC (Fig. 6). However, QaiD has significant cold bias, while ED has small warm bias (Fig. 6c,f), which are consistent with their spatial patterns shown in Fig. 2f-j. Significant warming trend over DNC is well captured by ERA5, but the warming trend in GTD is overestimated by 0.2℃/10a (Fig. 6b). For most sub-regions, ERA5 and OBS show better consistence after 2000, compared to the period 1979–2000.

Changes in annual precipitation in ERA5 and OBS have large differences in most sub-regions of DNC (Fig. 7). More importantly, the trends between these two datasets are divergent in some sub-regions. Based on the OBS, most of the sub-regions exhibit a wetting trend, expect for ED. In contrast, ERA5 show a drying trend in these sub-regions, except for QaiD. For ED, the decreasing trend in annual precipitation is − 6.9 mm/10a based on the OBS; however, this trend is severely overestimated in ERA5 (− 30.2 mm/10a). Finally, it is notable that the precipitation bias between these two datasets in most sub-regions is reduced after 2000, compared to the period 1979–2000.

4.2 Evaluation of climate extremes

The temperature extreme indices such as *TX*, *TN*, and *DTR* were calculated from OBS and ERA5, respectively (Fig. 8). *TX* values based on OBS vary greatly from the east to the west over DNC (Fig. 8a). For example, *TX* in TakD reaches to more than 20 ℃, while *TX* in Hulun Buir dune field is just around 6 ℃. QaiD has low *TX* due to its high altitude. ED and OrdosD have similar latitudes with TakD, but *TX* in ED and OrdosD is much lower. ERA5 well captures the spatial pattern of *TX*, but underestimates in about 90% of the

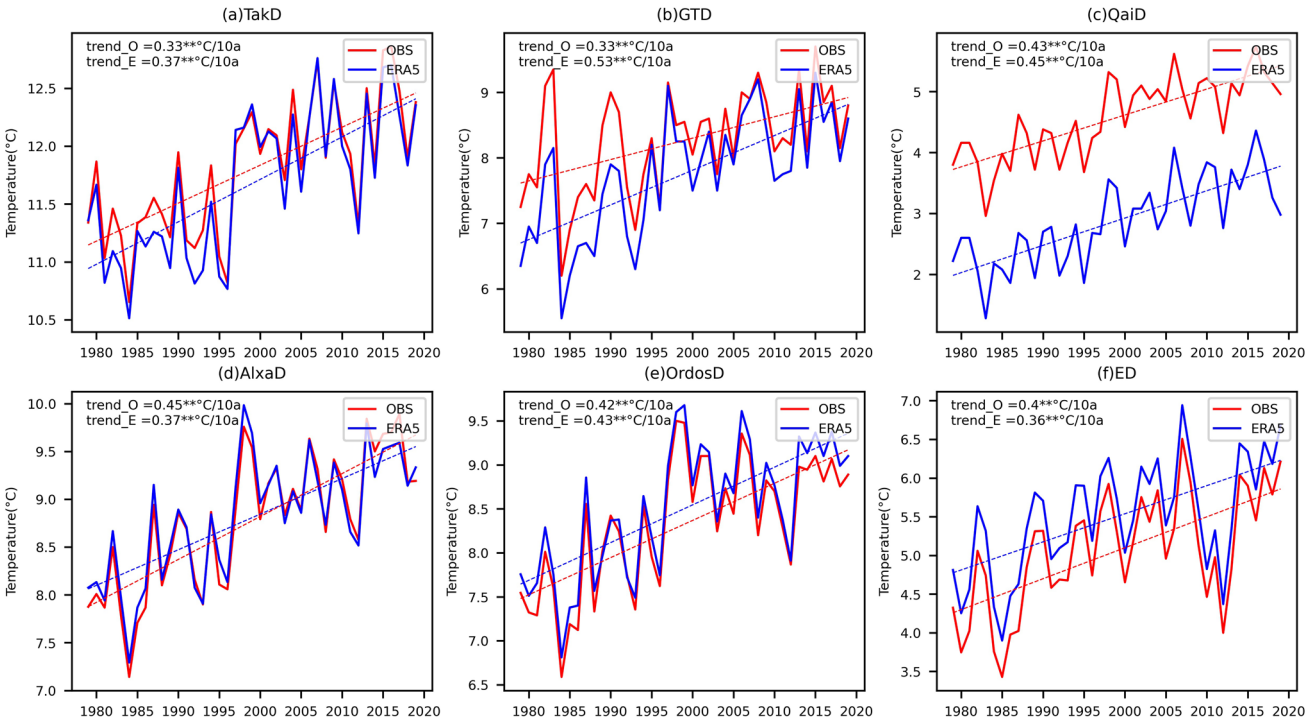

Fig. 6 Time series and linear trend of annual mean temperature based on the OBS and ERA5 during 1979–2019 over six sub-regions of DNC. The labels "trend_E" and "trend_O" indicate the trend calculated for ERA5 and OBS, respectively. The significant level of the trend was determined by Mann–Kendall test. Double and single asterisks indicate 99% and 95% significant levels, respectively

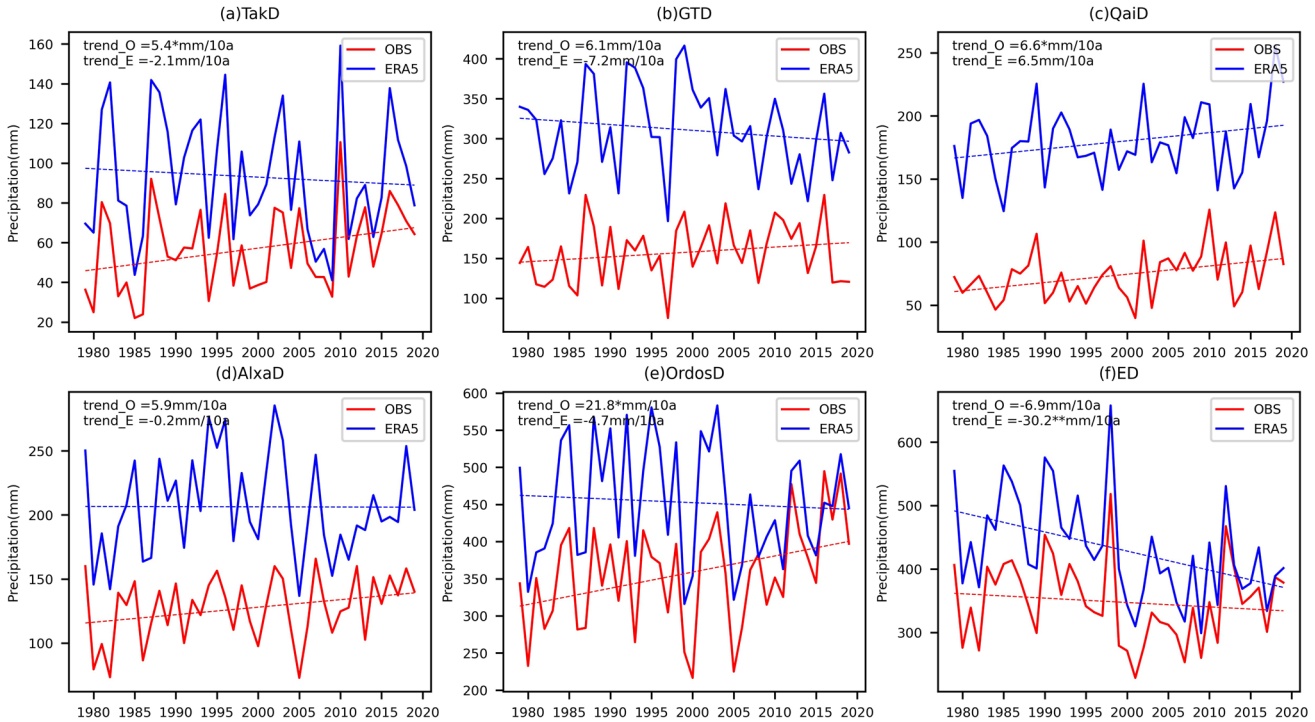

Fig. 7 Time series and linear trend of annual precipitation based on the OBS and ERA5 during 1979–2019 over six sub-regions of DNC. The labels "trend_E" and "trend_O" indicate the trend calculated for ERA5 and OBS, respectively. The significant level of the trend was determined by Mann–Kendall test. Double and single asterisks indicate 99% and 95% significant levels, respectively

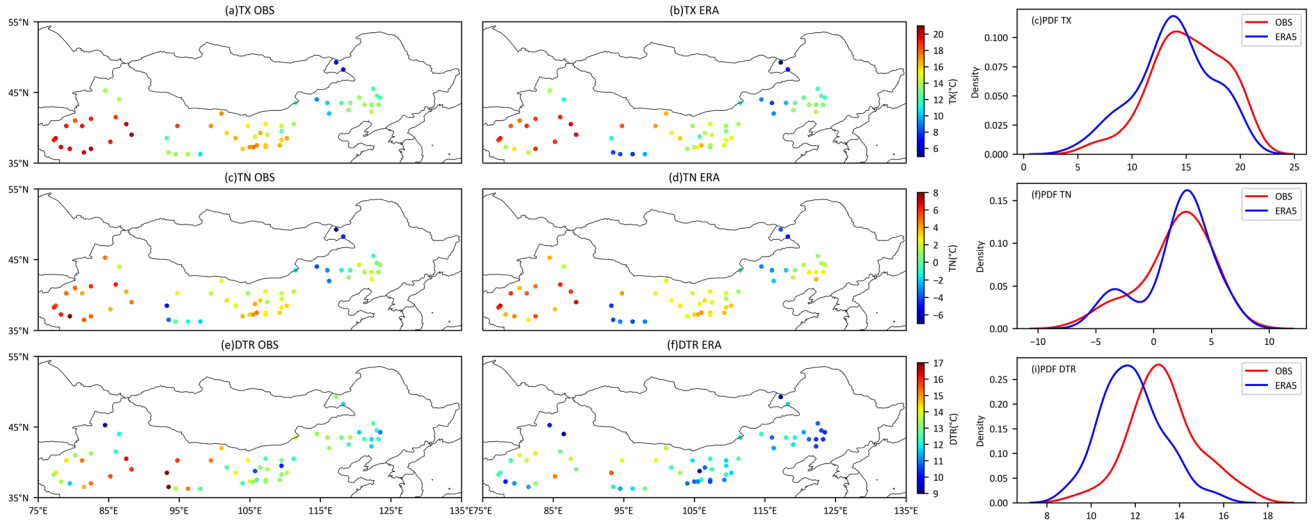

Fig. 8 Spatial distributions of three temperature extreme indices based on OBS and ERA5, respectively, and their probability density distribution (the rightmost panel). (**a**) *TX* calculated from OBS. (**b**) *TX* calculated from ERA5. (**c**) Probability density distribution of *TX* based on OBS and ERA5. (**d**) *TN* calculated from OBS. (**e**) *TN* calculated from ERA5. (**f**) Probability density distribution of *TX* based on OBS and ERA5. (**g**) *DTR* calculated from OBS. (**h**) *DTR* calculated from ERA5. (**i**) Probability density distribution of *DTR* based on OBS and ERA5

total stations (Fig. 8b). The comparison of the probability density distribution between OBS and ERA5 also reveals the underestimation of ERA5 in *TX* (Fig. 8c). Similar to *TX*, *TN* also shows large longitudinal variations across the DNC (Fig. 8d). *TN* in ED could reach to lower than − 6 ℃. In comparison, *TN* in TakD is around 5 ℃, much higher than

other sub-regions. ERA5 well captures the spatial pattern of *TN* (Fig. 8e), and no systematic bias is found between OBS and ERA5 (Fig. 8f). *DTR* in eastern TakD, QaiD, and AlxaD is higher than 15℃, while *DTR* in OrdosD and ED is mostly lower than 15 ℃ (Fig. 8g). The spatial pattern of *DTR* in ERA5 is similar to that of OBS (Fig. 8h). However, *DTR* is obviously underestimated by ERA5 (Fig. 8i), indicating the uncertainties in reproducing daily temperature variability by ERA5.

Interannual precipitation variability can be reflected by *CV*. In the relatively wet regions with annual precipitation around 200–450 mm, such as ED, OrdosD, and AlxaD, *CV* is below 0.3 (Fig. 9a), while *CV* in the driest TakD can reach to 0.7. Compared with the OBS, *CV* values in ERA5 are lower (Fig. 9c), especially in the driest TakD (Fig. 9b), indicating that ERA5 has low capacity to reproduce the precipitation variability in the study area. *SDII* indicates averaged precipitation intensity of all wet days (> 1 mm). As shown in Fig. 9d, *SDII* in ED can reach to 10 mm/day in the OBS. *SDII* in TakD is around 5 mm/day despite that the annual precipitation in this desert is less than 50 mm. *SDII* in ERA5 is generally lower than that of OBS across DNC (Fig. 9f). *Rx1d* (maximum 1-day precipitation) generally increase from west to east, and the maximum *Rx1d* reach to 70 mm in ED based on OBS (Fig. 9g). In ERA5, the *Rx1d* values are slightly lower than that of OBS (Fig. 9i). *CDD* is calculated by maximum number of consecutive days with precipitation < 1 mm. According to OBS, *CDD* in TakD can reach to more than 150 days (Fig. 9j), while *CDD* in ED and OrdosD is around 40–100 days. *CDD* calculated based on ERA5 is much lower than the OBS (Fig. 9l). *RD* (number of days with precipitation no lower than 1 mm) also shows a decreasing trend from east to west and range from 0 to 60 days based on the OBS (Fig. 9m). However, *RD* in ERA5 is much higher than that of OBS (Fig. 9o).

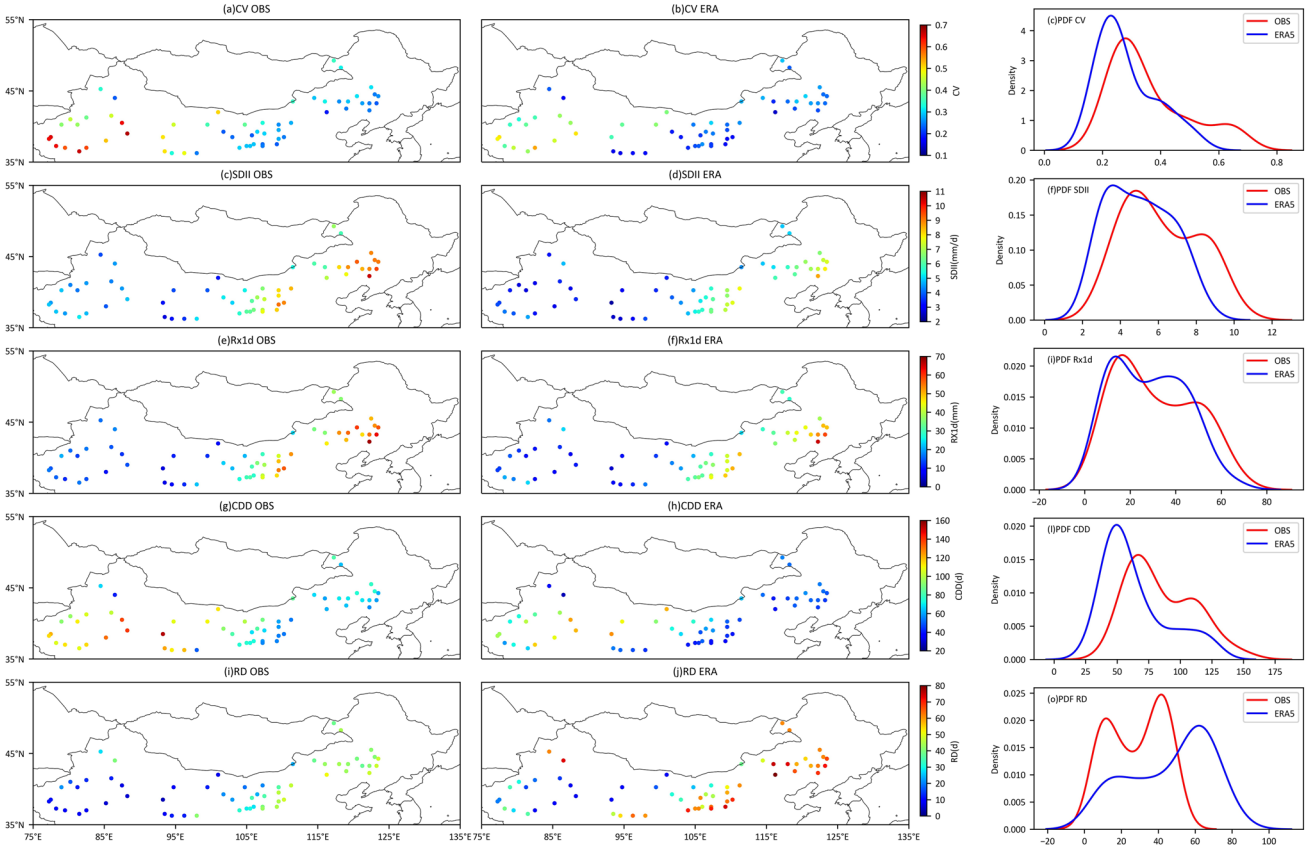

Fig. 9 Spatial distributions of five precipitation extreme indices based on OBS and ERA5, respectively, and their probability density distribution (the rightmost panel). (**a**) *CV* calculated from OBS. (**b**) *CV* calculated from ERA5. (**c**) Probability density distribution of *CV* based on OBS and ERA5. (**d**) *SDII* calculated from OBS. (**e**) *SDII* calculated from ERA5. (**f**) Probability density distribution of *SDII* based on OBS and ERA5. (**g**) *Rx1d* calculated from OBS. (**h**) *Rx1d* calculated from ERA5. (**i**) Probability density distribution of *Rx1d* based on OBS and ERA5. (**j**) *CDD* calculated from OBS. (**k**) *CDD* calculated from ERA5. (**l**) Probability density distribution of *CDD* based on OBS and ERA5. (m) *RD* calculated from OBS. (**n**) *RD* calculated from ERA5. (**o**) Probability density distribution of *RD* based on OBS and ERA5

4.3 Evaluation of detection skills of daily precipitation

The performance of daily precipitation in ERA5 was examined by *POD*, *FAR*, and *CSI* (Fig. 10). The averaged *POD* of daily precipitation over DNC as a whole is 0.74, which means that 74% of observed daily precipitation are detected by ERA5. *POD* in some parts of TakD and AlxaD is as low as 0.5 (Fig. 10a). The averaged *FAR* over DNC as a whole is 0.66. High *FAR* is mostly distributed in TakD and QaiD (Fig. 10b), where the annual precipitation is severely overestimated (Fig. 2f). Finally, the averaged *CSI* over DNC as a whole is 0.30. The regions with high *CSI* are generally consistent with the regions with relatively high *POD* and low *FAR* in the eastern part of DNC, such as ED and OrdosD (Fig. 10c).

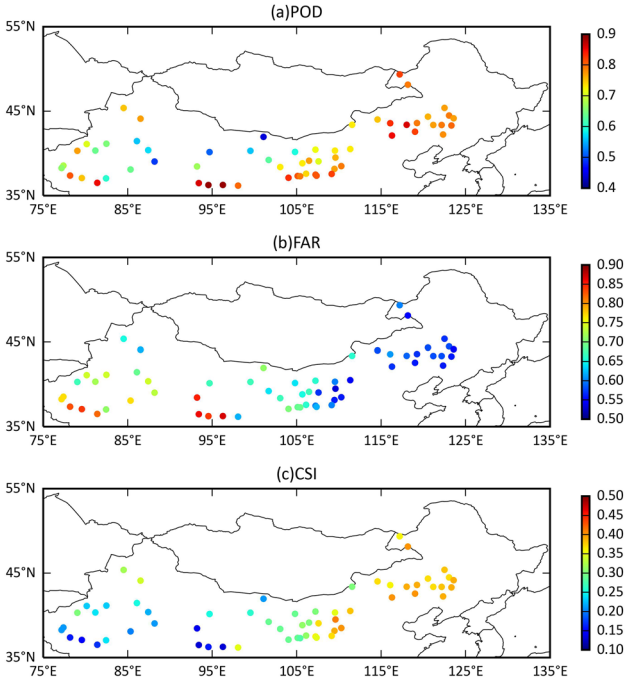

Fig. 10 Spatial distribution of daily precipitation indices that used to evaluate the capacity of ERA5 in detecting daily precipitation events. **a** Probability of detection (*POD*). **b** False alarm ratio (*FAR*). **c** Critical success index (*CSI*)

5 Discussion

5.1 The performance of ERA5 in comparison with other precipitation datasets

Overall, based on the comparison between ERA5 and ground observations, this study finds that ERA5 performs well in reproducing the spatial–temporal variations of annual and seasonal temperatures over DNC. However, relatively large bias exits in reproducing the annual precipitation and precipitation extremes. To further evaluate the quality of ERA5 and to make up for the uncertainties of precipitation and precipitation extremes over DNC, some other reanalysis and gridded gauge-based precipitation datasets were analyzed in comparison with ERA5. The other four reanalysis datasets include MERRA2, NCEP1, NCEP2, and NOAA-20C, and the gridded gauge-based precipitation datasets are PREC/L, GPCP, and CPC. Most of these datasets have the same time span as ERA5, except for MERRA2 with time span of 1980–2019 and NOAA-20C with time span of 1979–2015. The results (Table 5) show that ERA5 yielded the highest *CC*, lowest *RB*, and lowest *RRMSE* in annual precipitation among all five reanalysis products. Ren et al. (2022) have compared the performance of reanalysis datasets in Central Asia, and their results show that in comparison to ERA5, MERRA2 has higher correlation and lower deviation with gauge-based precipitation datasets. Jiang et al. (2021) have compared ERA5 with gauge-based precipitation datasets from 2003 to 2015 and also found that ERA5 has relatively high biases in precipitation estimates. However, they also note that the performance of ERA5 in precipitation estimates varies significantly across different sub-regions of mainland China. It further indicates that the performance of reanalysis

Table 5 Evaluation results of reanalysis and gridded gauge-based precipitation datasets for annual precipitation and daily precipitation detection skills

Datasets		Statistic indices			Daily precipitation detection capacity		
		CC	*RB* (%)	*RRMSE*	*POD*	*FAR*	*CSI*
Reanalysis datasets	ERA5	0.65	61.4	0.76	0.74	0.66	0.30
	MERRA2	0.53	66.3	0.95	\		
	NCEP1	0.43	186.2	2.27	0.32	0.84	0.11
	NCEP2	0.43	85.6	1.37	0.24	0.81	0.11
	NOAA-20C	0.46	159.7	1.73	0.54	0.84	0.14
Gridded precipitation datasets	PREC/L	0.70	17.6	0.42	\		
	GPCP	0.55	60.4	0.80	\		
	CPC	0.71	13.7	0.38	0.36	0.80	0.15

datasets could be different in different regions. Nevertheless, in our study area, gauge-based precipitation datasets (PREC/L, GPCP, and CPC) have lower *RB* and *RRMSE* than ERA5. Previous studies have pointed out that because gauge-based precipitation datasets integrate more ground observations, they usually have higher accuracy than reanalysis and satellite-based precipitation datasets (Schiemann et al. 2008; Wei et al. 2021). Despite that, ERA5 has the advantage in detecting daily precipitation events with the highest *POD* (0.85) among all reanalysis and gauge-based precipitation datasets in the study area. ERA5 also has the lowest *FAR* (0.66) and highest *CSI* (0.30) compared with other precipitation datasets.

As for precipitation extremes, these reanalysis datasets have different performance in reproducing different extreme indices. The gauge-based precipitation dataset CPC shows the best performance (Table 6). Among the reanalysis datasets, ERA5 has the highest *CC* and lowest *RRMSE* in reproducing these extreme indices, but the relative bias of *CV*, *SDII*, and *CDD* is higher than that of other reanalysis datasets. The advantage of ERA5 compared with other reanalysis datasets in precipitation extremes is consistent with previous studies (i.e., Zhu et al. 2017). Nevertheless, these results provide a reference for dataset selection when investigating certain precipitation extreme indices in the study area.

5.2 Possible causes for the temperature and precipitation bias in ERA5

As mentioned above, the ERA5 has different performances in reproducing the annual and seasonal variations, climate extremes, and detection skills of daily precipitation in the deserts and dune fields of northern China. Previous studies have indicated that the bias in reanalysis datasets may be caused by several factors (Huang et al. 2016), and the differences between datasets may additionally be related to different data sources, prediction models, initial conditions, bias correction methods, and data assimilation systems (Smith et al. 2001). Here, the possible causes for temperature and precipitation bias in ERA5 are briefly discussed based on current analysis in DNC.

Temperature in the reanalysis products is often one of the most reliable variables (Kalnay et al. 1996), but it tends to be underestimated in high-altitude regions (Zhao et al. 2008; Liu et al. 2018). Our results confirm that the annual temperature estimates in ERA5 have cold bias as high as 3 °C in the high-altitude Qaidam desert (Fig. 2f). The underestimation of temperature could be related to low simulation skills of climate models in complex terrains or caused by the difference between the terrain height used in the reanalysis data and the actual height of weather stations (Wang et al. 2015).

The spatial distribution of temperature extremes is well reproduced by ERA5 (Fig. 8); however, biases still exist in

Table 6 Evaluation results of reanalysis and gridded gauge-based precipitation datasets for precipitation extremes

Datasets		*CV*			*SDII*			*Rx1d*			*CDD*			*RD*		
		CC	*RB* (%)	*RRMSE*	*CC*	*RB* (%)	*RRMSE*	*CC*	*RB* (%)	*RRMSE*	*CC*	*RB* (%)	*RRMSE*	*CC*	*RB* (%)	*RRMSE*
Reanalysis datasets	ERA5	0.82	−21.4	0.31	0.43	−18.6	0.34	0.34	−7.1	0.59	0.36	−25.2	0.42	0.56	80.8	0.91
	NCEP1	0.22	−9.6	0.42	0.21	−7.90	0.37	0.14	−13.8	0.70	0.20	−14.7	0.50	0.42	169.5	1.98
	NCEP2	0.45	4.9	0.36	0.18	−3.60	0.38	0.14	−13.8	0.69	0.28	−3.70	0.47	0.45	71.7	1.12
	NOAA-20C	0.61	−46.7	0.56	0.27	−43.7	0.52	0.20	−46.2	0.71	0.18	−25.0	0.56	0.44	153.8	1.73
Gridded precipitation dataset	CPC	0.92	2.1	0.18	0.62	−18.2	0.32	0.54	−16.1	0.54	0.57	−4.0	0.31	0.58	29.8	0.47

their relative magnitude. The underestimation of *TX* and overestimation of *TN* seems a common problem in reanalysis products and climate models (Mao et al. 2010; Li et al. 2022). For example, Mahto and Mishra (2019) have found that ERA5 underestimates seasonal maximum temperature with a bias of − 0.3 ℃ and overestimates minimum temperature with a bias of 0.6 ℃ in Indian during monsoon seasons. You et al. (2013) have suggested that both NCEP/NCAR and ERA-Interim reanalysis have underestimated the annual extreme high temperature in China by − 0.23% and − 0.17%, respectively, while the annual extreme low temperature is overestimated by 0.26% and 0.16%, respectively. Even using regional climate model and dynamical downscaling of reanalysis, there might be still considerable cold bias of *TX* and warm bias of *TN* (Zhang et al. 2009; Heikkilä et al. 2011). Based on this study, we suspect that the bias in ERA5 could be even larger in the desert regions. The diurnal temperature change in the deserts could be rapid due to low heat capacity of land surface (Malek and Bingham 1997), and as a result, the temperature extremes would have low occurrence probability and not easily be captured by model simulations. Because the temperature extremes often have an important impact on ecological and hydrological processes in the deserts, such biases should be carefully considered when integrating the ERA5 reanalysis into ecological or hydrological models.

The precipitation may have even larger uncertainty than temperature in ERA5, probably due to the complex precipitation process and limited model ability to describe this process (Smith et al. 2001). In this study, both annual and seasonal precipitations are overestimated by ERA5 across DNC. The underestimation of coefficient of variation (*CV*) indicates that EAR5 may fail to reproduce the large variability of precipitation in the desert areas. The performance of ERA5 in reproducing precipitation extremes is not as good as gauge-based precipitation datasets (Table 6). The drawbacks could be caused by the overestimation of rainfall occurrence in ERA5 (Nogueira 2020; Jiang et al. 2021). Indeed, this study shows that ERA5 has relatively higher *RD* (Fig. 9), indicating that there are more rainy days in ERA5 compared to the OBS, and high *FAR* is found especially in the drier western part of DNC (Fig. 10b). The bias of daily precipitation of different grades is further analyzed, and it is clear that ERA5 has significantly overestimated the daily precipitation of 0.1–1 mm and of 1–2 mm in the study area (Fig. 11). By contrast, daily precipitation of 5–10 mm and 10–20 mm is largely underestimated. The overestimation of 0.1–1 mm daily precipitation could result in higher *RD* and *FAR* in ERA5, while the underestimation of relatively strong daily precipitation (5–10, 10–20 mm) may lead to lower precipitation intensity (*SDII*). The precipitation uncertainty seems a common problem in reanalysis products. For

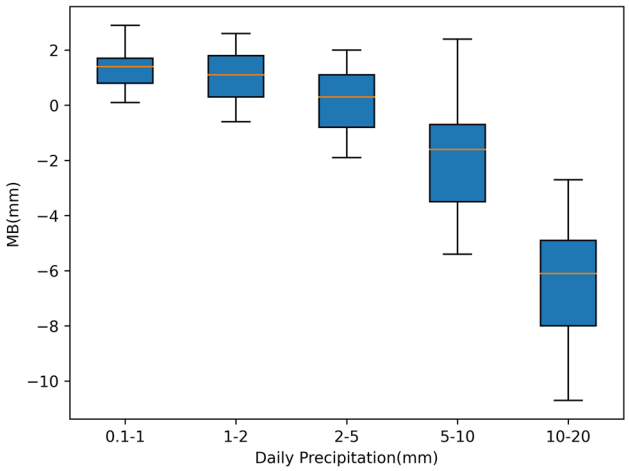

Fig. 11 Boxplot of mean bias calculated for daily precipitation of different grades in ERA5

instance, ERA-Interim largely overestimates the number of wet days but fails to report strong rainfall events (Soares et al. 2012). Heikkilä et al. (2011) suggest that the overestimation of light precipitation in climate models may lead to the uncertainty of wet days and daily precipitation intensity. Several studies have indicated that assimilation of more observations in the model may help to reduce the uncertainty of precipitation estimates in the reanalysis products (Kalnay et al. 1996; Zhang et al. 2012). Furthermore, the wet biases are especially obvious near the mountains in the study area, such as southern Taklamakan desert, Gurban Tunggut desert, Qaidam desert, and southern Tengger desert (Fig. 4f). The complex terrains with large topographic gradient have significantly dynamical and thermal impacts on local climate (Ma et al. 2009; Palazzi et al. 2013). The poor representation of complex topography in the models may lead to the uncertainty in precipitation simulation (Zhang et al. 2013; Wang et al. 2020).

Last but not least, the rapid warming trend in DNC during the last few decades has been well reproduced by the ERA5, but there are apparently divergent trends in precipitation between the OBS and ERA5 (Fig. 7). We suspect that such biases may be due to the data assimilation methods used in reanalysis, which generally reduce random errors in time series but may also introduce a fictitious trend (Trenberth et al. 2003; Bengtsson 2004). Indeed, ERA5 has smaller precipitation variability in the study area, compared to the OBS. Nevertheless, caution is needed when evaluating the long-term climate trend using the reanalysis data. Moreover, the deviation of both temperature and precipitation in ERA5 has been reduced after 2000 (Figs. 6 and 7), partially due to more available ground observations assimilated in the climate reanalysis in the twenty-first century (Bengtsson et al.

2007). Therefore, it can image that the accuracy of reanalysis data would be further improved by assimilating more ground observations and more available satellite data in the future.

6 Conclusions

In the study, we examined the performance of ERA5 reanalysis over DNC by comparing with the ground observations as well as other datasets, focusing on annual and seasonal temperatures and precipitations, climate extremes, and detection skills of daily precipitation. The conclusions can be summarized as follows.

ERA5 well captures the observed spatial pattern of annual and seasonal temperatures with correlation coefficient greater than 0.9. However, cold bias greater than − 3 ℃ exists in high-altitude regions, such as the Qaidam desert. Both annual and seasonal precipitations are overestimated across DNC, and the relative bias of annual, summer, and winter precipitations are 65%, 40%, and 194% respectively. Overall, ERA5 reproduces well the warming trend over DNC during the past four decades, but divergent trends in precipitation are found between ERA5 and the observations.

As for climate extremes, both daily maximum temperature and daily temperature range are underestimated by ERA5. The interannual precipitation variability, precipitation intensity, maximum 1-day precipitation, and the number of continuous dry days are underestimated, while the number of the rainy days is largely overestimated by ERA5. ERA5 can detect more than 70% observed rainy days over DNC, but the false alarm ratio is 66% over the whole DNC and is as high as 90% in drier regions such as Taklamakan desert and Qaidam desert. It is found that ERA5 has different biases in reproducing daily precipitation of different grades and may lead to the uncertainty of precipitation estimates. More specifically, the overestimation of light precipitation may result in more rainy days and higher precipitation in ERA5, while the underestimation of strong daily precipitation (5–10, 10–20 mm) may lead to lower precipitation intensity, in comparison to the observations.

Although ERA5 still has some uncertainties in reproducing both temperature and precipitation over DNC, it outperforms other reanalysis datasets in the study area. Gridded gauge-based precipitation datasets show better performance in reproducing precipitation and precipitation extremes over DNC. This study provides an important reference for the use of ERA5 reanalysis over DNC and also insights for other observation-limited desert regions in the world.

Acknowledgements We gratefully acknowledge the China Meteorological Data Service Center for the supply of meteorological data. And we thank the ECMWF, NOAA, and NASA for the reanalysis datasets and gauge-based precipitation datasets. We appreciate the helpful and constructive comments by the reviewers.

Author contribution Zhiwei Xu and Danqing Huang collected the data, conceptualized, and lead the project. Chengzhi Hou analyzed the data and wrote the draft. All authors contributed to the interpretation of the results and revised the paper.

Funding This study was supported by the National Natural Science Foundation of China (Nos. 41871012, 42075020), the Regional Key Program of Science and Technology Development Plan (Nos. 2022E01014, 2019BFG02024), the Fundamental Research Funds for the Central Universities of China (0209–14380091), and the Chinese Academy of Sciences Interdisciplinary Innovation Team.

Data availability The ground observation data were derived from China Meteorological Administration (http://cdc.cma.gov.cn/). ERA5 reanalysis data were obtained from the Copernicus Climate Data Store (https://cds.climate.copernicus.eu/#!/home). NCEP1, NCEP2, NOAA-20C, PREC/L, and CPC data are derived from the NOAA Physical Sciences Laboratory (https://psl.noaa.gov/data/gridded/index.html), MERRA2 is derived from the National Aeronautics and Space Administration Goddard Space Flight Center (https://disc.gsfc.nasa.gov/datasets/M2TMNXFLX_5.12.4/summary), and GPCP is derived from the Global Precipitation Climatology Project (https://www.ncei.noaa.gov/data/global-precipitation-climatology-project-gpcp-monthly/access/).

Code availability The programs used to generate all the results are Python 3.8 and ArcGIS 10.8.

Declarations

Ethics approval Not applicable.

Consent to participate Not applicable.

Consent for publication Not applicable.

Competing interests The authors declare no competing interests.

References

Albergel C, Dutra E, Munier S, Calvet J, Munoz-Sabater J, de Rosnay P, Balsamo G (2018) ERA-5 and ERA-Interim driven ISBA land surface model simulations: which one performs better? Hydrol Earth Syst Sci 22(6):3515–3532

Bengtsson L, Arkin P, Berrisford P, Bougeault P, Folland CK, Gordon C, Haines K, Hodges KI, Jones P, Kallberg P, Rayner N, Simmons AJ, Stammer D, Thorne PW, Uppala S, Vose RS (2007) The need for a dynamical climate reanalysis. Bull Am Meteor Soc 88(4):495–502

Bengtsson L (2004) Can climate trends be calculated from reanalysis data? *Journal of Geophysical Research*, 109(D11)

Bergametti G, Rajot JL, Pierre C, Bouet C, Marticorena B (2016) How long does precipitation inhibit wind erosion in the Sahel? Geophys Res Lett 43(12):6643–6649

Bosilovich MG (2013) Regional climate and variability of NASA MERRA and recent reanalyses: U.S summertime precipitation and temperature. J Appl Meteorol Climatol 52(8):1939–1951

Bosilovich MG, Chen J, Robertson FR, Adler RF (2008) Evaluation of global precipitation in reanalyses. J Appl Meteorol Climatol 47(9):2279–2299

Charney JG (1975) Dynamics of deserts and drought in the Sahel. Q J R Meteorol Soc 101:193–202

Chen M, Xie P, Janowiak JE, Arkin PA (2002) Global land precipitation: a 50-yr monthly analysis based on gauge observations. J Hydrometeorol 3(3):249–266

Dinku T, Ceccato P, Cressman K, Connor SJ (2010) Evaluating detection skills of satellite rainfall estimates over desert locust recession regions. J Appl Meteorol Climatol 49(6):1322–1332

Donat MG, Sillmann J, Wild S, Alexander LV, Lippmann T, Zwiers FW (2014) Consistency of temperature and precipitation extremes across various global gridded in situ and reanalysis datasets. J Clim 27(13):5019–5035

Giese BS, Seidel HF, Compo GP, Sardeshmukh PD (2016) An ensemble of ocean reanalyses for 1815–2013 with sparse observational input. J Geophys Res: Oceans 121(9):6891–6910

Graham RM, Hudson SR, Maturilli M (2019) Improved performance of ERA5 in arctic gateway relative to four global atmospheric reanalyses. Geophys Res Lett 46(11):6138–6147

He Q, Jin L (2021) Summary of meteorological field experiments in the Taklimakan Desert, China. J Xinjiang Univ (Nat Sci Ed Chinese Eng) 38(3):334–354

Heikkilä U, Sandvik A, Sorteberg A (2011) Dynamical downscaling of ERA-40 in complex terrain using the WRF regional climate model. Clim Dyn 37(7–8):1551–1564

Hersbach H, Bell B, Berrisford P, Hirahara S, Horányi A, Muñoz Sabater J, Nicolas J, Peubey C, Radu R, Schepers D, Simmons A, Soci C, Abdalla S, Abellan X, Balsamo G, Bechtold P, Biavati G, Bidlot J, Bonavita M, Chiara G, Dahlgren P, Dee D, Diamantakis M, Dragani R, Flemming J, Forbes R, Fuentes M, Geer A, Haimberger L, Healy S, Hogan RJ, Hólm E, Janisková M, Keeley S, Laloyaux P, Lopez P, Lupu C, Radnoti G, Rosnay P, Rozum I, Vamborg F, Villaume S, Thépaut JN (2020) The ERA5 global reanalysis. Q J R Meteorol Soc 146(730):1999–2049

Hodges KI, Lee RW, Bengtsson L (2011) A Comparison of extratropical cyclones in recent reanalyses ERA-Interim, NASA MERRA, NCEP CFSR, and JRA-25. J Clim 24(18):4888–4906

Huai B, Wang J, Sun W, Wang Y, Zhang W (2021) Evaluation of the near-surface climate of the recent global atmospheric reanalysis for Qilian Mountains. Qinghai-Tibet Plateau Atmospheric Research 250:105401

Huang D, Zhu J, Zhang Y, Huang Y, Kuang X (2016) Assessment of summer monsoon precipitation derived from five reanalysis datasets over East Asia. Q J R Meteorol Soc 142(694):108–119

Huang J, Ma J, Guan X, Li Y, He Y (2019) Progress in semi-arid climate change studies in China. Adv Atmos Sci 36(9):922–937

Huang J, Yin J, Wang M, He Q, Guo J, Zhang J, Liang X, Xie Y 2021 Evaluation of five reanalysis products with radiosonde observations over the central Taklimakan Desert during summer. *Earth and Space Science*, 8(5).

Huffman GJ, Adler RF, Arkin P, Chang A, Ferraro R, Gruber A, Janowiak J, McNab A, Rudolf B, Schneider U (1997) The Global Precipitation Climatology Project (GPCP) combined precipitation dataset. Bull Am Meteor Soc 78(1):5–20

Jiang Q, Li W, Fan Z, He X, Sun W, Chen S, Wen J, Gao J, Wang J (2021) Evaluation of the ERA5 reanalysis precipitation dataset over Chinese Mainland. J Hydrol 595:125660

Kalnay E, Kanamitsu M, Kistler R, Collins W, Deaven D, Gandin L, Iredell M, Saha S, White G, Woollen J, Zhu Y, Chelliah M, Ebisuzaki W, Higgins W, Janowiak J, Mo KC, Ropelewski C, Wang J, Leetmaa A, Reynolds R, Jenne R, Joseph D, Less V (1996) The NCEP/NCAR 40-year reanalysis project. Bull Am Meteor Soc 77(3):437–472

Kampf SK, Faulconer J, Shaw JR, Lefsky M, Wagenbrenner JW, Cooper DJ (2018) Rainfall thresholds for flow generation in desert ephemeral streams. Water Resour Res 54(12):9935–9950

Kanamitsu M, Ebisuzaki W, Woollen J, Yang SK, Hnilo JJ, Fiorino M, Potter G (2002) NCEP-DOE AMIP-II reanalysis (R-2). *Bulletin of the American Meteorological Society*, 1631–1643.

Kim D, Chin M, Remer LA, Diehl T, Bian H, Yu H, Brown ME, Stockwell WR (2017) Role of surface wind and vegetation cover in multi-decadal variations of dust emission in the Sahara and Sahel. Atmos Environ 148:282–296

Kucharski F, Zeng N, Kalnay E (2013) A further assessment of vegetation feedback on decadal Sahel rainfall variability. Clim Dyn 40(5–6):1453–1466

Li G, Yang H, Zhang Y, Huang C, Pan X, Ma M, Song M, Zhao H (2019) More extreme precipitation in Chinese deserts from 1960 to 2018. Earth and Space Science 6(7):1196–1204

Li X, Yuan C, Hang J (2022) Heat wave trends in Southeast Asia: comparison of results from observation and reanalysis data. *Geophysical Research Letters*, 49(4)

Liu Z, Liu Y, Wang S, Yang X, Wang L, Baig MHA, Chi W, Wang Z (2018) Evaluation of spatial and temporal performances of ERA-Interim precipitation and temperature in Mainland China. J Clim 31(11):4347–4365

Liu J, Shangguan D, Liu S, Ding Y, Wang S, Wang X (2019) Evaluation and comparison of CHIRPS and MSWEP daily-precipitation products in the Qinghai-Tibet Plateau during the period of 1981–2015. Atmos Res 230:104634

Ma L, Zhang T, Frauenfeld OW, Ye B, Yang D, Qin D (2009) Evaluation of precipitation from the ERA-40, NCEP-1, and NCEP-2 reanalyses and CMAP-1, CMAP-2, and GPCP-2 with ground-based measurements in China. *Journal of Geophysical Research*, 114(D9)

Mahto SS, Mishra V (2019) Does ERA-5 outperform other reanalysis products for hydrologic applications in India? Journal of Geophysical Research: Atmospheres 124(16):9423–9441

Malek E, Bingham GE (1997) Partitioning of radiation and energy balance components in an inhomogeneous desert valley. J Arid Environ 37(2):193–207

Mao J, Shi X, Ma L, Kaiser DP, Li Q, Thornton PE (2010) Assessment of reanalysis daily extreme temperatures with China's homogenized historical dataset during 1979–2001 using probability density functions. J Clim 23(24):6605–6623

Ning WX, Liu XY, Wang ZT (2021) Temperature and precipitation characteristics and spatial stratified heterogeneity in Badain Jaran Desert (in Chinese). J Univ Chinese Acad Sci 38(01):103–113

Nogueira M (2020) Inter-comparison of ERA-5, ERA-interim and GPCP rainfall over the last 40 years: process-based analysis of systematic and random differences. J Hydrol 583:124632

Palazzi E, von Hardenberg J, Provenzale A (2013) Precipitation in the Hindu-Kush Karakoram Himalaya: observations and future scenarios. J Geophys Res: Atmospheres 118(1):85–100

Peel MC, Finlayson BL, McMahon TA (2007) Updated world map of the Köppen-Geiger climate classification. Hydrol Earth Syst Sci 11:1633–1644

Ren Y, Yu H, Liu C, He Y, Huang J, Zhang L, Hu H, Zhang Q, Chen S, Liu X, Zhang M, Wei Y, Yan Y, Fan W, Zhou J (2022) Attribution of dry and wet climatic changes over Central Asia. J Clim 35(5):1399–1421

Schiemann R, Lüthi D, Vidale PL, Schär C (2008) The precipitation climate of Central Asia—intercomparison of observational and numerical data sources in a remote semiarid region. Int J Climatol 28(3):295–314

Smith SR, Legler DM, Verzone KV (2001) Quantifying uncertainties in NCEP reanalyses using high-quality research vessel observations. J Clim 14(20):4062–4072

Soares PMM, Cardoso RM, Miranda PMA, de Medeiros J, Belo-Pereira M, Espirito-Santo F (2012) WRF high resolution dynamical downscaling of ERA-Interim for Portugal. Clim Dyn 39(9–10):2497–2522

Su J, Wang J, Li H, Shang K, Kang Y, Jia X, Wu Z (2016) Preliminary analysis of precipitation characteristics in the Badain Jaran

and Tengger Desert (in Chinese). Journal of Arid Meteorology 34(02):261–268

Thomas DSG, Shaw PA (1991) 'Relict' desert dune systems: interpretations and problems. J Arid Environ 20:1–14

Torralba V, Doblas-Reyes FJ, Gonzalez-Reviriego N (2017) Uncertainty in recent near-surface wind speed trends: a global reanalysis intercomparison. Environ Res Lett 12(11):114019

Trenberth KE, Dai A, Rasmussen ROYM, Parsons DB (2003) The changing character of precipitation. Bull Am Meteor Soc 84(9):1205–1217

Wang S, Zhang M, Sun M, Wang B, Huang X, Wang Q, Feng F (2015) Comparison of surface air temperature derived from NCEP/DOE R2, ERA-Interim, and observations in the arid northwestern China: a consideration of altitude errors. Theoret Appl Climatol 119(1–2):99–111

Wang X, Hua T, Lang L, Ma W (2017) Spatial differences of aeolian desertification responses to climate in arid Asia. Global Planet Change 148:22–28

Wang S, Yu Y, Zhang X, Lu H, Zhang X, Xu Z (2021) Weakened dust activity over China and Mongolia from 2001 to 2020 associated with climate change and land-use management. Environ Res Lett 16(12):124056

Wang L, Qiu Y, Han Z, Xu C, Wu S, Wang Y, Holmgren M, Xu Z (2022) Climate, topography and anthropogenic effects on desert greening: a 40-year satellite monitoring in the Tengger desert, northern China. CATENA 209:105851

Wang Y, Yang K, Zhou X, Chen D, Lu H, Ouyang L, Chen Y, Lazhu, Wang B, Naturvetenskapliga F, Faculty OS, Göteborgs U, Institutionen F G, Gothenburg U 2020 Department, O. E. S. Synergy of orographic drag parameterization and high resolution greatly reduces biases of WRF-simulated precipitation in central Himalaya. *Climate dynamics*, 54(3-4): 1729-1740

Wei L, Jiang S, Ren L, Wang M, Zhang L, Liu Y, Yuan F, Yang X (2021) Evaluation of seventeen satellite-, reanalysis-, and gauge-based precipitation products for drought monitoring across mainland China. Atmos Res 263:105813

Xie P, Chen M, Yang S, Yatagai A, Hayasaka T, Fukushima Y, Liu C (2007) A gauge-based analysis of daily precipitation over East Asia. J Hydrometeorol 8(3):607–626

Xu Z, Hu R, Wang K, Mason JA, Wu S, Lu H (2018) Recent greening (1981–2013) in the Mu Us dune field, north-central China, and its potential causes. Land Degrad Dev 29(5):1509–1520

You Q, Fraedrich K, Min J, Kang S, Zhu X, Ren G, Meng X (2013) Can temperature extremes in China be calculated from reanalysis? Global Planet Change 111:268–279

Zhang Y, Dulière V, Mote PW, Salathé E (2009) Evaluation of WRF and HadRM mesoscale climate simulations over the US Pacific Northwest. J Clim 22(20):5511–5526

Zhang Q, Körnich H, Holmgren K (2013) How well do reanalyses represent the southern African precipitation? Clim Dyn 40(3–4):951–962

Zhang S, Wang D, Qin Z, Zheng Y, Guo J (2018) Assessment of the GPM and TRMM precipitation products using the rain gauge network over the Tibetan Plateau. Journal of Meteorological Research 32:324–335

Zhang L, Kumar A, Wang W (2012) Influence of changes in observations on precipitation: a case study for the Climate Forecast System Reanalysis (CFSR). *Journal of Geophysical Research: Atmospheres*, 117(D08105).

Zhao T, Guo W, Fu C (2008) Calibrating and evaluating reanalysis surface temperature error by topographic correction. J Clim 21(6):1440–1446

Zhu J, Huang D, Yan P, Huang Y, Kuang X (2017) Can reanalysis datasets describe the persistent temperature and precipitation extremes over China? Theoret Appl Climatol 130(1–2):655–671